Available online at www.sciencedirect.com
SCIENCE DIRECT®
Journal of Computational Physics 185 (2003) 562–582
JOURNAL OF COMPUTATIONAL PHYSICS
www.elsevier.com/locate/jcp

Anisotropy, propagation failure, and wave speedup in traveling waves of discretizations of a Nagumo PDE ☆

Christopher E. Elmer [a,*], Erik S. Van Vleck [b]

[a] *Department of Mathematical Sciences. New Jersey Institute of Technology, Newark, NJ 07102, USA*
[b] *Department of Mathematics, University of Kansas, Lawrence, KS 66045, USA*

Received 4 March 2002; received in revised form 20 October 2002; accepted 20 December 2002

Abstract

This article is concerned with effect of spatial and temporal discretizations on traveling wave solutions to parabolic PDEs (Nagumo type) possessing piecewise linear bistable nonlinearities. Solution behavior is compared in terms of waveforms and in terms of the so-called (a, c) relationship where a is a parameter controlling the bistable nonlinearity by varying the potential energy difference of the two phases and c is the wave speed of the traveling wave. Uniform spatial discretizations and $A(\alpha)$ stable linear multistep methods in time are considered. Results obtained show that although the traveling wave solutions to parabolic PDEs are stationary for only one value of the parameter a, a_0, spatial discretization of these PDEs produce traveling waves which are stationary for a nontrivial interval of a values which include a_0, i.e., failure of the solution to propagate in the presence of a driving force. This is true no matter how wide the interface is with respect to the discretization. For temporal discretizations at large wave speeds the set of parameter a values for which there are traveling wave solutions is constrained. An analysis of a complete discretization points out the potential for nonuniqueness in the (a, c) relationship.

Keywords: Bistable partial differential equation; Traveling waves; Spatial and temporal discretization

1. Introduction

Reaction–diffusion, Ginzburg–Landau, Allen–Cahn equations, or more generally time-dependent partial differential equations (PDEs) that contain a reaction, or driving term, along with a spatial dispersion term, are fundamental tools for the modeling of many physical systems. The simplest solutions to these equations are constant solutions at the equilibrium values of the reaction term. If the nonlinearity possesses at least two equilibrium points one can consider solutions that "connect" different equilibrium points. These

☆ The work of E.S.V.V. was supported in part by NSF Grants DMS-9973393 and DMS-0139824. The work of C.E.E. was supported in part by NSF Grant DMS-0204573.
* Corresponding author.
E-mail addresses: elmer@m.njit.edu (C.E. Elmer), evanvleck@math.ukans.edu (E.S. Van Vleck).

0021-9991/03/$ - see front matter © 2003 Published by Elsevier Science B.V.
doi:10.1016/S0021-9991(03)00004-4

heteroclinic connections may correspond to traveling wave solutions which are often very stable solutions of the PDE. In particular, for the case of bistable nonlinearities, traveling wave solutions connecting the two "stable" equilibria attract a large class of initial conditions (see [2,13]).

Our contribution in this paper is to consider the effect of discretization (both spatial and temporal) on the behavior of traveling wave solutions to bistable PDEs with piecewise linear nonlinearities. We find that the effect of spatial discretization is most evident for wave speed $c \approx 0$, while for temporal discretization changes are most evident for large wave speeds. Our results may serve to benchmark the effect of such discretization and may be useful in understanding the impact of truncation from the infinite spatial domains considered here to finite domains with various boundary conditions. When approximating solutions to partial differential equations in a neighborhood of traveling wave solutions, we consider finite differences in space and stiffly stable methods in time. Our approach is to consider the resulting differential-difference equations (for a semi-discretization) or the resulting difference equations (for a complete discretization), apply a traveling wave ansatz, and then analyze the resulting traveling wave equations. The traveling wave equations of the discretized equations exhibit fundamentally different solution characteristics and wave speed properties compared to the traveling wave equations of the PDE. Included are phenomena such as the shape of the solution profile being step-like instead of tanh-like (corresponding to lurching in the motion of the interface) (occurring in both the time and space discretizations), failure of the interface to propagate (space discretization), anisotropy in the speed of interface dependent on the spatial discretization, and speed up of the wave (time discretization). An example from materials science where these characteristics affect the robustness of numerical studies is phase-field modeling [31] of phase transitions, where the continuous transition between any two phases (the interface) is a thin layer with thickness of order less than or equal to the underlying mesh used in the numerics [3,30]. Interface speed up, pinning, and anisotropic interface movement all occur when using finite difference methods to study the time evolution of phase field models. This paper points out that care needs to be taken to be sure that these effects are minimal in such numerical phase field studies.

There has been much work on the existence and stability of monotone traveling wave solutions of bistable reaction–diffusion PDEs, notably the work of Fife and McLeod [13] and Aronson and Weinberger [2]. In addition, work on traveling wave solutions of spatially discrete bistable equations has been motivated by the importance of these types of equations as models in their own right (see for example [5,9,17–19,34,35]). Recently, there has been interest in equations of the form of mixed-type delay equations characterized by having both backward and forward delays (see the work of Mallet-Paret [20,21]) that occur when considering the traveling wave equations for such spatially discrete systems. Notable work related to time discretization includes that of Weinberger [33,34] and that of Chow et al. [4] that considers (up to rescaling) a uniform in space, forward Euler in time complete discretization. In this paper we consider more appropriate time-stepping techniques, $A(\alpha)$ stable linear multistep methods. The time-stepping techniques we consider here are the so-called regular methods (see, e.g., [27]) that do not add or subtract equilibrium solutions, hence we will not expect to see pinning or propagation failure due to time discretization.

We consider the Nagumo PDE [23]

$$u_t = \epsilon^2 \Delta u - f(u), \tag{1}$$

where $u \equiv u(x,t)$, $x \in \mathbb{R}^n$ for $n = 1, 2$, or 3, Δ is the standard Laplacian operator, $t \geqslant 0$ and f is a bistable piecewise linear nonlinearity (see [12,22,26,28,29])

$$f(u) \equiv \begin{cases} u, & u < a, \\ u - 1, & u > a, \\ [a-1, a], & u = a, \end{cases} \tag{2}$$

where $0 < a < 1$ is a so-called detuning parameter. Results for smooth nonlinearities such as $u(u-1)(u-a)$ can be found in [11]. A traveling wave solution is a pair (φ, c) satisfying $\varphi(x \cdot \sigma - ct) = u(x,t)$, where $\sigma \in \mathbb{R}^n$

satisfies $||\sigma||_2 = 1$ and specifies the direction in which the plane wave is propagating. The function φ determines the profile of the wave and c determines the wave speed. The so-called traveling wave equation that must be satisfied for (1) is

$$-c\dot{\varphi}(\xi) = \epsilon^2\ddot{\varphi}(\xi) - f(\varphi(\xi)), \quad \xi \equiv x\cdot\sigma - ct \in \mathbb{R}, \tag{3}$$

together with the boundary conditions $\varphi(-\infty) = 0$ and $\varphi(+\infty) = 1$. Observe that the traveling wave equation (3) is independent of the dimension n, is independent of the direction of propagation σ, and is unique only up to translation.

Using the techniques in [6,8], one can show that for (3) with the nonlinearity (2), φ is the C^1 function

$$\varphi(\xi) = \frac{1}{2} + \frac{1}{\pi}\int_0^\infty \frac{A(s)\sin(s\xi)\,\mathrm{d}s}{s(A^2(s)+c^2s^2)} + \frac{c}{\pi}\int_0^\infty \frac{\cos(s\xi)\,\mathrm{d}s}{A^2(s)+c^2s^2} = H(\xi) + C_\pm \mathrm{e}^{\lambda_\pm \xi}, \quad \xi \in \mathbb{R}, \tag{4}$$

where $A(s) = 1+\epsilon^2 s^2, H(\xi)$ is the Heaviside step function,

$$C_\pm = \begin{cases} \frac{1}{2} + \frac{c}{2\sqrt{4\epsilon^2+c^2}}, & \xi \leqslant 0, \\ -\frac{1}{2} + \frac{c}{2\sqrt{4\epsilon^2+c^2}}, & \xi \geqslant 0, \end{cases} \quad \text{and} \quad \lambda_\pm = \begin{cases} \frac{-c+\sqrt{4\epsilon^2+c^2}}{2\epsilon^2}, & \xi \leqslant 0, \\ \frac{-c-\sqrt{4\epsilon^2+c^2}}{2\epsilon^2}, & \xi \geqslant 0, \end{cases}$$

and the relationship between the wave speed c and the detuning parameter a is given by

$$a = \frac{1}{2} + \frac{c}{\pi}\int_0^\infty \frac{\mathrm{d}s}{A^2(s)+c^2s^2} = \frac{1}{2} + \frac{c}{2\sqrt{4\epsilon^2+c^2}}, \tag{5}$$

where because φ is monotone we have chosen the unique translate such that $\varphi(0) = a$. We remark here that the piecewise linear nonlinearity is a prototype of a smooth nonlinearity with the property that $\lim_{a\to 1} c(a) = +\infty$; as opposed to the cubic nonlinearities $\varphi(\varphi-a)(\varphi-1)$ or $\varphi(\varphi^2-1)+F(\varphi,a)$, which are often considered, where $\lim_{a\to 1} c(a) = [c^*,+\infty)$ for some finite value c^*. The piecewise linear nonlinearity has the added advantage that it facilitates the use of transform techniques so we are able to obtain a good deal of information about the solution behavior of both the PDE system and the discretized systems.

The outline of this paper is as follows. In Section 2 we consider uniform rectangular spatial discretizations and point out changes in solution behavior due to anisotropy in the difference approximation to the Laplacian and the inability of the difference operator to resolve steep fronts resulting in pinning or failure of the wave to propagate. We consider temporal discretization with $A(\alpha)$ stable linear multistep methods in Section 3 and focus on BDF methods which are the methods of choice in codes such as DASSL [24,25] and LSODE [16] for the solution of stiff differential equations. Initially we present the form of the traveling wave equations which are retarded differential-difference equations (see [15]), and subsequently state theorems proving the existence of monotone traveling wave solutions for the Backward Euler temporal discretization with piecewise linear bistable reaction term. We exhibit explicit forms for the traveling wave solutions with the piecewise linear reaction term and for the Backward Euler discretization find the error to first approximation in the wave form and the (a,c) curve in Section 4. In Section 5 we consider the error in the (a,c) curves in the limits as $|c| \to \infty$ for temporal discretizations and as $c \to 0$ for spatial discretizations. We find that characteristics of the limiting behaviors in the (a,c) curves for semidiscretizations occur for all c for the complete discretization, in fact the (a,c) are set valued for a dense set of values of c. Section 6 contains our conclusions.

2. Spatial discretization and traveling waves

We now consider the spatial discretization of (1) with mesh widths of $\Delta x_i,\ i = 1,\ldots,n$, in the coordinate directions, thus obtaining a spatially discrete equation of the form

$$\begin{aligned}\frac{\mathrm{d}U_j(t)}{\mathrm{d}t} &= \epsilon^2 LU_j(t) - f(U_j(t)),\\ LU_j(t) &= \sum_{i=1}^{n}\left\{\frac{1}{\Delta x_i^2}[U_{j+e_i}(t) + U_{j-e_i}(t) - 2U_j(t)]\right\},\end{aligned} \tag{6}$$

with $U_j(t) \approx u(j\Delta x, t)$ with $j\Delta x = [j_1\Delta x_1, \ldots, j_n\Delta x_n]$, where $j \in \mathbb{Z}^n$ and e_i is the ith unit vector. For (6) the traveling wave equations are $(\varphi(j\Delta x \cdot \sigma - ct) = U_j(t))$

$$-c\dot{\varphi}(\xi) = \epsilon^2 L_T\varphi(\xi) - f(\varphi(\xi)), \quad \xi \equiv j\Delta x \cdot \sigma - ct \in \mathbb{R}, \tag{7}$$

$$L_T\varphi(\xi) = \sum_{i=1}^{n}\left\{\frac{1}{\Delta x_i^2}[\varphi(\xi + \Delta x_i\sigma_i) + \varphi(\xi - \Delta x_i\sigma_i) - 2\varphi(\xi)]\right\}$$

together with the boundary conditions $\varphi(-\infty) = 0$ and $\varphi(+\infty) = 1$.

Formulas for the waveform and detuning parameter for (7) with f, (2), are found by replacing $A(s)$ with

$$\tilde{A}(s) = \tilde{A}(x, \{\Delta x_i\}_{i=1}^n) := 1 + 2\sum_{i=1}^{n}\frac{\epsilon^2}{\Delta x_i^2}(1 - \cos(s\Delta x_i\sigma_i)) \tag{8}$$

in (4) and (5), respectively. The transform techniques used to find these solutions are justified by the arguments in [6]. We mention here that as opposed to the traveling wave equations for the PDE (3) the traveling wave equations for the spatial discretization (7) depend on the spatial dimension n and direction of propagation σ. This is simply due to the fact that the Laplacian is isotropic (direction independent) while the finite difference operator is anisotropic [6–8]. In addition, as will demonstrated in Section 5, a major difference [17,18,21,35] between the behavior of traveling wave solutions for PDE and the spatial discretization is the existence of a range of a about 1/2 for which the wave speed $c = 0$.

We consider rectangular spatial meshes because they are the first step in analyzing the existence and behavior of traveling wave solutions of Nagumo PDEs under discretization and because such spatially discrete systems have been proposed as models of biological and physical systems. In general, for static nonuniform spatial discretizations we do not expect to have monotone traveling wave solutions due to the requirement of translation invariance. A study of nonuniform discretizations that move with the traveling wave would be interesting, but is beyond the scope of this work.

3. Linear multistep methods and traveling wave solutions

Next we consider time discretization schemes for the PDE (1), apply an appropriate traveling wave ansatz, and then analyze the resulting traveling wave equations. Consider the application of a consistent linear multistep method (see [14]) to the differential equation $\dot{u} = g(u)$. The resulting difference equation has the form $\sum_{j=0}^{k}\alpha_j U_{n+j} = \Delta t\sum_{j=0}^{k}\beta_j g(U_{n+j})$, where $U_{n+j} \approx u(t_{n+j})$ and Δt is the temporal step size. In particular, for (1) we obtain

$$\sum_{j=0}^{k}\alpha_j U_{n+j}(x) = \Delta t\sum_{j=0}^{k}\beta_j[\epsilon^2\Delta U_{n+j}(x) - f(U_{n+j}(x))]. \tag{9}$$

The traveling wave ansatz becomes $\Psi(x\cdot\sigma - ct_k) = U_k(x)$ which upon substitution into (9) yields the traveling wave equations

$$\sum_{j=0}^{k}\alpha_j\Psi(\xi - jc\Delta t) = \Delta t\sum_{j=0}^{k}\beta_j\left[\epsilon^2\ddot{\Psi}(\xi - jc\Delta t) - f(\Psi(\xi - jc\Delta t))\right], \quad \xi = x\cdot\sigma - ct_0 \in \mathbb{R}. \tag{10}$$

3.1. Temporal discretization: linear multistep methods

Our interest is in monotone solutions Ψ which for the nonlinearity (2) allows for a simplification to a linear inhomogeneous equation. If Ψ is monotone and we choose the translate such that $\Psi(0) = a$, then for the piecewise linear f as in (2), $f(\Psi(\xi)) = \Psi(\xi) - H(\Psi(\xi) - a) = \Psi(\xi) - H(\xi)$, where H is the Heaviside function. In this case (10) becomes

$$\sum_{j=0}^{k}\alpha_j\Psi(\xi - jc\Delta t) = \Delta t\sum_{j=0}^{k}\beta_j[\epsilon^2\ddot{\Psi}(\xi - jc\Delta t) - \Psi(\xi - jc\Delta t) + H(\xi - jc\Delta t)]. \tag{11}$$

Due to stiffness considerations we focus on $A(\alpha)$ stable linear multistep methods, in particular, on stable BDF methods (see [14]). Much of our analysis with the piecewise linear f in (2) will depend on the smoothness of the solution Ψ and in general we do not expect that the second derivative will be continuous but it may be regarded as set valued at a finite number of points. Because $\beta_k \neq 0$ while $\beta_j = 0$ for $j = 0,\ldots,k-1$ for the BDF methods

$$\ddot{\Psi}(0+) - \ddot{\Psi}(0-) = \frac{1}{\epsilon^2}. \tag{12}$$

In the following theorem, whose proof is found in [10], monotonicity of the wave form is assumed for the piecewise linear f.

Theorem 1. *Consider the application of a linear multistep method to* (1) *with f given by* (2). *For* $\Delta t > 0$, *if* $\sum_{j=0}^{k}\alpha_j = 0$ *and*

$$\sum_{j=0}^{k}\exp(-\mathrm{i}jc\Delta t s)(\alpha_j/\Delta t + \beta_j A(s)) \neq 0, \quad A(s) = \epsilon^2 s^2 + 1, \tag{13}$$

in the horizontal strip $-\delta \leqslant \mathrm{Im}\, s \leqslant 0$ *for small* $\delta > 0$, *then there exists a solution* Ψ *to* (10) *satisfying* $\Psi(-\infty) = 0$ *and* $\Psi(+\infty) = 1$ *of the form*

$$\Psi(\xi) = \frac{1}{2} + \frac{1}{\pi}\int_0^\infty \frac{D(s,\Delta t,\xi)\,\mathrm{d}s}{sE(s,\Delta t)}, \tag{14}$$

where

$$D(s,\Delta t,\xi) = \left\{\sum_{l=1}^{k}\sum_{j=0}^{k-l}[\beta_j c_{j+l}\sin(s\xi + lc\Delta t s) + c_j\beta_{j+l}\sin(s\xi - lc\Delta t s)] + \sum_{j=0}^{k}\beta_j c_j\sin(s\xi)\right\}, \tag{15}$$

$$E(s,\Delta t) = \sum_{l=1}^{k}\sum_{j=0}^{k-l}[2c_j c_{j+l}\cos(lc\Delta t s)] + \sum_{j=0}^{k}c_j^2, \tag{16}$$

where $d = c\Delta t$, *and* $c_j = \alpha_j/\Delta t + \beta_j(\epsilon^2 s^2 + 1) = \alpha_j/\Delta t + \beta_j A(s)$.

Remark 3.1. In [10] it is shown that for the Backward Euler discretization the condition (13) in Theorem 1 is satisfied. For higher-order BDF methods we were not able to justify the monotonicity assumption due to the lack of smoothness observed in Eqs. (12). It is also possible to show (see [10]) that for the Backward Euler discretization of (1) for $c \neq 0$, the curve $c(a)$ is strictly monotone.

3.2. Complete discretization – Backward Euler and rectangular spatial mesh

If we consider a Backward Euler discretization in time and standard second-order finite differences for the spatial discretization, then the traveling wave equation for the complete discretization is

$$-\Psi(\xi) + \Psi(\xi - c\Delta t) = \Delta t[\epsilon^2 L_T \Psi(\xi - c\Delta t) - f(\Psi(\xi - c\Delta t))], \tag{17}$$

where L_T is given in (7). In this case the formula for the waveform and the (a, c) relationship may be obtained from (14) and (18), respectively, by replacing c_j with $\tilde{c}_j = \alpha_j/\Delta t + \beta_j \tilde{A}(s)$ for $j = 0, 1$ in (15), (16), and (18), where $\tilde{A}(s)$ is as defined in (8). The justification of the monotonicity assumption follows from the results in [6] and the results on the Backward Euler method in this section.

4. Leading order error analysis

For the piecewise linear reaction term f we obtain a relationship between the wavespeed c and the detuning parameter a by setting $\xi = 0$ for monotone waves assuming $\varphi(0) = \Psi(0) = a$.

4.1. Error analysis – linear multistep methods

For the consistent linear multistep methods

$$a = \Psi(0) = \frac{1}{2} + \frac{1}{\pi}\int_0^\infty \frac{\tilde{D}(s,\Delta t)\,\mathrm{d}s}{sE(s,\Delta t)}, \quad \tilde{D}(s,\Delta t) = \sum_{l=1}^{k}\sum_{j=0}^{k-l}(\beta_j c_{j+l} - c_j\beta_{j+l})\sin(lc\Delta t s). \tag{18}$$

Using the formulas obtained for the PDE (4) and (5) and for the linear multistep discretizations (14) and (18) we determine expressions for the error in the waveform and the difference in a as functions of ϵ, Δt, and c.

To determine the error in a for fixed values of ϵ, Δt, and c consider

$$\mathrm{Err}_a = |\varphi(0) - \Psi(0)| = \left|\frac{1}{\pi}\int_0^\pi \frac{c}{A^2(s) + c^2 s^2} - \frac{\tilde{D}(s,\Delta t)}{sE(s,\Delta t)}\,\mathrm{d}s\right| = \left|\tilde{C}_1\Delta t + \tilde{C}_2\Delta t^2 + \cdots\right|, \tag{19}$$

where

$$\tilde{\Gamma}(s,\Delta t) \equiv \frac{\tilde{D}(s,\Delta t)}{sE(s,\Delta t)} \quad \text{and} \quad \tilde{C}_n = \frac{1}{n!}\frac{1}{\pi}\int_0^\infty \frac{\partial^n \tilde{\Gamma}(s,0)}{\partial \Delta t^n}\,\mathrm{d}s,$$

for $n = 1, 2, 3, \ldots$ Similarly, for the error in the waveform at arbitrary $\xi \in \mathbb{R}$ consider

$$\mathrm{Err}_\varphi(\xi) = \left|C_1\Delta t + C_2\Delta t^2 + \cdots\right|, \tag{20}$$

where

$$\Gamma(s,\Delta t,\xi) \equiv \frac{D(s,\Delta t,\xi)}{sE(s,\Delta t)} \quad \text{and} \quad C_n \equiv C_n(\xi) = \frac{1}{n!}\frac{1}{\pi}\int_0^\infty \frac{\partial^n \Gamma(s,0,\xi)}{\partial \Delta t^n}\,\mathrm{d}s,$$

for $n = 1, 2, 3, \ldots$ By a direct calculation we obtain the following theorem.

Theorem 2. *For a consistent linear multistep method the coefficient $C_1(\xi)$ is given by*

$$C_1(\xi) = -\frac{1}{3\pi}\Lambda(\alpha,\beta)\frac{1}{\epsilon^8}\left\{c^2\left[I^s_{20}(\xi)+2\epsilon^2 I^s_{21}(\xi)+\epsilon^4 I^s_{22}(\xi)\right]+c^3\left[I^c_{21}(\xi)+\epsilon^2 I^c_{22}(\xi)\right]\right\} \tag{21}$$

and

$$\tilde{C}_1 = C_1(0) = -\frac{1}{3\pi}\Lambda(\alpha,\beta)\frac{c^3}{\epsilon^8}[I_{21}+\epsilon^2 I_{22}], \tag{22}$$

where the integrals I_{ij}, $I^c_{ij}(\xi)$, $I^s_{ij}(\xi)$ are tabulated in Appendix A *and*

$$\Lambda(\alpha,\beta) = -\frac{1}{3}\left[\sum_{j=0}^{k}\beta_j\right]^2\Bigg/\left[\sum_{j=0}^{k}\sum_{l=0}^{k}(j-l)^2\beta_l\alpha_j\right].$$

As a corollary to Theorem 2 we have the following for the Backward Euler method.

Corollary 4.1. *For the Backward Euler method $\Lambda(\alpha,\beta)=3$, and*

$$C_1(\xi) = -\frac{c}{4(c^2+4\epsilon^2)^{3/2}}\left[c^2\left(e^{-\sqrt{-\alpha_2}|\xi|}+e^{-\sqrt{-\alpha_1}|\xi|}\right)+4\epsilon^2\left(e^{-\sqrt{-\alpha_2}|\xi|}-e^{-\sqrt{-\alpha_1}|\xi|}\right)+\left(\frac{c+\sqrt{c^2+4\epsilon^2}}{2\epsilon^2}e^{-\sqrt{-\alpha_1}|\xi|}\right.\right.$$
$$\left.\left.+\frac{c-\sqrt{c^2+4\epsilon^2}}{2\epsilon^2}e^{-\sqrt{-\alpha_2}|\xi|}+\sqrt{-\alpha_1}e^{-\sqrt{-\alpha_2}|\xi|}+\sqrt{-\alpha_2}e^{-\sqrt{-\alpha_1}|\xi|}\right)\frac{\sqrt{c^2+4\epsilon^2}}{2}\xi\right],$$

where

$$\alpha_1 = \frac{-(c^2+2\epsilon^2)+c\sqrt{c^2+4\epsilon^2}}{2\epsilon^4} \quad \textit{and} \quad \alpha_2 = \frac{-(c^2+2\epsilon^2)-c\sqrt{c^2+4\epsilon^2}}{2\epsilon^4},$$

and

$$\tilde{C}_1 = C_1(0) = -\frac{c^3}{2(c^2+4\epsilon^2)^{3/2}}.$$

4.2. Error analysis – rectangular spatial discretization

To determine the manner in which the error in the relationship between the detuning parameter a and the wavespeed c depends on the mesh widths $\{\Delta x_i\}_{i=1}^n$ under a spatial semidiscretization we expand in a Taylor series in Δx. We find that the leading order terms are Δx_i^2 terms and if we let $\hat{C}_i$ denote the coefficient multiplying Δx_i^2 we have

$$\hat{C}_i = -\frac{1}{\pi}\int_0^\infty \frac{(\partial^2\tilde{A}/\partial\Delta x_i^2)(s,0)\sin(s\xi)}{s(A^2(s)+c^2s^2)}\,ds+\frac{2}{\pi}\int_0^\infty \frac{A^2(s)(\partial^2\tilde{A}/\partial\Delta x_i^2)(s,0)\sin(s\xi)}{s(A^2(s)+c^2s^2)^2}\,ds$$
$$+\frac{2c}{\pi}\int_0^\pi \frac{A(s)(\partial^2\tilde{A}/\partial\Delta x_i^2)(s,0)\cos(s\xi)}{(A^2(s)+c^2s^2)^2}\,ds$$
$$= -\frac{c}{3\epsilon^6\pi}\left[I_{22}+\epsilon^2 I_{23}\right], \tag{23}$$

where the values of I_{22}, I_{23} are tabulated in Appendix A. After some calculation we find that the leading order terms for the error in a, Err_a, are of the form

$$\mathrm{Err}_a = -\frac{c(c^2+6\epsilon^2)}{24\epsilon^2(c^2+4\epsilon^2)^{3/2}}\left[\sum_{i=1}^{n}\sigma_i^4\Delta x_i^2\right]+\cdots. \tag{24}$$

Hence given a direction of propagation σ the choice of spatial discretization with $\sigma_i^4\Delta x_i^2 = \text{const}$ for $i = 1,\ldots,n$ gives, to leading order, equal contributions to the error in a.

4.3. Error analysis – complete discretization

If we combine the error analysis for the Backward Euler temporal discretization and the spatial discretization we find that to leading order the error in a has the form

$$\mathrm{Err}_a = -\frac{c}{2(c^2+4\epsilon^2)^{3/2}}\left[c^2\Delta t+\frac{(c^2+6\epsilon^2)}{12\epsilon^2}\sum_{i=1}^{n}\sigma_i^4\Delta x_i^2\right]+\cdots. \tag{25}$$

This provides, to leading order, ratios of the time-step Δt and the spatial mesh that for a given wave speed c and diffusion coefficient ϵ^2 equally distribute the error in a between the temporal discretization and the temporal discretization.

5. The behavior of a as $|c|$ approaches 0 or ∞

When solving the traveling wave equations (3) and (7) and their approximations (10) and (17) for a given c we also find the value of the detuning parameter a. The functions $a(c)$ for (3) are monotone and have range $(0,1)$ for nonlinearity (2). With the boundary conditions $\varphi(-\infty) = \Psi(-\infty) = 0$ and $\varphi(+\infty) = \Psi(+\infty) = 1$ we now examine the $a(c)$ curves for each of our discretized examples and in particular we examine the error in a, Err_a, with particular attention to the cases $|c| \to \infty$ and $|c| \to 0$, when using these various approximation methods. As $|c| \to \infty$, the second derivative and second-order difference terms, the terms that come from the diffusion operator, will go to zero. Thus any error in a, or the solution curve, comes from the temporal discretization. As $|c| \to 0$, the first derivative and the first-order difference terms, the terms that come from the time derivative, will go to zero. Thus any error in a, or the solution curve, comes from the spatial discretization.

5.1. The numerical method

In the following sections we include plots of the solution profiles and the $a(c)$ relations. All four of of our traveling wave equations (3), (10), (7), and (17), with f (2), can be written as

$$G(\bar{v}, a) = 0, \tag{26}$$

where $\bar{v} = \{v(x),\ldots,v(x-kc\Delta t), v(x+\Delta x_1\sigma_1),\ldots,v(x+\Delta x_1\sigma_1 - kc\Delta t),\ldots,v(x-\Delta x_n\sigma_n - kc\Delta t)\}$ with boundary conditions $v(-\infty) = 0$, $v(\infty) = 1$. For all but (17), Eq. (26) is a two-point boundary value problem on an infinite interval that is transitionally invariant. For any numerical representation of (26) there exists a continuous nonlinearity f which has exactly the same values of (2) everywhere the nonlinearity is evaluated. Hence we can treat (26) as nonlinear and consider its linearization. Since we are solving for both v and a we consider the variation of (26) with respect to v and a which is

$$G_{\bar{v}}(\bar{v}, a)\bar{w} + G_a(\bar{v}, a)b = 0,$$

which has the isolated solution $w = d\dot{v}$ and $b = \dot{a} = 0$ for any $d \in \mathbb{R}$. Thus, we add to (26) the condition $\dot{a} = 0$. When solving (17), we add a $\varepsilon\dot{v}$ term and take $\varepsilon \to 0\pm$. We used an experimental collocation based boundary value problem solver for functional differential equations of mixed type [1] using appropriate boundary functions defined in terms of eigenfunctions of the linearization about 0 and 1 to truncate the infinite interval. Results where obtained by computing in double precision, compiled with True64 Fortran, and run on a Compaq/DEC Alpha chip.

5.2. Spatial discretization of Eq. (3)

To determine Err_a we consider the (a, c) relationship for (3) and for (7). In the infinite wavespeed limit the spatial derivatives and differences no longer effect the solution profile or the value of a. In the zero wave speed limit however, behavior of the solution profile or the value of a are fundamentally different, exhibiting propagation failure and step-like profiles, phenomena not present in the PDE.

5.2.1. Spatial discretization in the $|c| \to \infty$ limit

Theorem 3. *When using* (7) *to approximate* (3), *in the limit* $|c| \to \infty$ *the* $\mathrm{Err}_a \to 0$.

Proof. Assume $c > 0$ and $\Delta t > 0$ and let $\phi(\eta) = \varphi(\xi)$ with $\eta = \xi/c$. Then (3) and (7), respectively, become

$$-\dot{\phi}(\eta) = \frac{\epsilon^2}{c^2}\ddot{\phi}(\eta) - f(\phi(\eta)), \quad -\dot{\phi}(\eta) = \epsilon^2 L_\infty \phi(\eta) - f(\phi(\eta)), \tag{27}$$

where

$$L_\infty \phi(\eta) = \sum_{i=1}^{n} \left\{ \frac{1}{\Delta x_i^2} \left[\phi\left(\eta + \frac{\Delta x_i}{c}\sigma_i\right) + \phi\left(\eta - \frac{\Delta x_i}{c}\sigma_i\right) - 2\phi(\eta) \right] \right\}.$$

Defining $\phi_*(\eta) \equiv \lim_{c\to\infty} \phi(\eta, c)$, for $\ddot{\phi}(\eta) < \infty$, $\sum_{i=1}^{n} \Delta x_i \neq 0$, $\eta \in \mathbb{R}$, $\lim_{c\to\infty} \epsilon^2/c^2 = 0$, $\lim_{c\to\infty} L_\infty \phi(\eta) = 0$, Eqs. (27) with (2) both become

$$\dot{\phi}_*(\eta) = f(\phi_*(\eta)), \quad \text{thus } \phi_*(\eta) = \begin{cases} \mathrm{e}^{\eta}, & \eta \leqslant 0, \\ 1, & \eta > 0, \end{cases}$$

$a = 1$, $\mathrm{Err}_a = 0 = \mathrm{Err}_{\phi_*}(\eta)$, and there is a jump discontinuity in $\dot{\phi}_*$ at 0. Similarly, when $c < 0$, we can define $\phi_*(\eta) \equiv \lim_{c\to-\infty} \phi(\eta, c)$ Eq. (27) with (2) both become

$$\dot{\phi}_*(\eta) = -f(\phi_*(\eta)), \quad \text{thus } \phi_*(\eta) = \begin{cases} 0, & \eta \leqslant 0, \\ 1 - \mathrm{e}^{-\eta}, & \eta > 0, \end{cases}$$

$a = 0$ with no error in a or the solution curve and there is a jump discontinuity in $\dot{\phi}_*$ at 0. □

Fig. 1(a) shows the $a(c)$ curves for these two cases. Observe the behavior in the tails.

5.2.2. Spatial discretization in the $|c| \to 0$ limit

The details and proofs of the following results for (7) with (2) were first developed in [6]. We begin with some notation. Real numbers ω_1, ω_2 are said to be rationally independent if for $j, k \in \mathbb{Z}$, $j \cdot \omega_1 + k \cdot \omega_2 = 0$ if and only if $j = k = 0$. If for any $j \neq k$, and k and $j = 1, \ldots, n$, $\Delta x_j \sigma_j$ and $\Delta x_k \sigma_k$ are rationally independent, then we say we have a rationally independent spatial discretization, we say we have a rationally dependent spatial discretization otherwise. Let $\varphi_*(\xi) \equiv \lim_{c\to 0} \varphi(\xi, c)$.

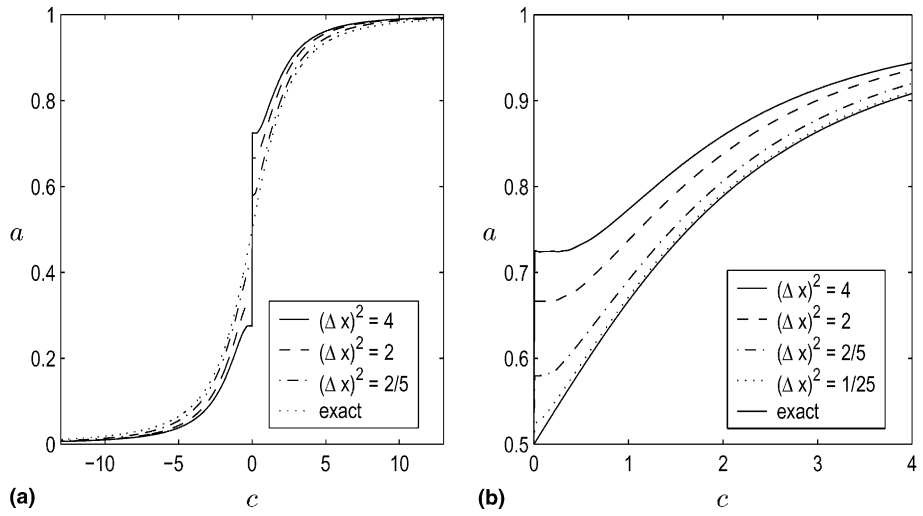

Fig. 1. Plots of $a(c)$ for the spatial discretization with piecewise linear f. Plot (a) shows that the error occurs near $c = 0$. Plot (b) is an enlargement of Plot (a).

Theorem 4. *We have the following*:

(*a*) *The limit defining* $\varphi_*(\xi)$ *exists pointwise.*

(*b*) $\varphi_*(\xi)$ *is defined almost everywhere on* $\mathbb{R}$, *but can contain jump discontinuities, in fact if the spatial discretization is rationally dependent* $\varphi_*(\xi)$ *consists of a countable discrete set of values in* $[0,1]$ (*the solution consists of piecewise constant functions*).

Theorem 5. *We have the following*:

(*a*) *Setting* $\varphi(0,c) = a$ *we find*

$$\varphi_\pm = \lim_{c\to 0^\pm} \varphi(0,c) = \frac{1}{2} \pm \lim_{T\to\infty} \frac{1}{2T} \int_0^T \frac{\mathrm{d}s}{\tilde{A}(s)}, \tag{28}$$

where $\tilde{A}(s)$ *is defined by* (8). *Thus, there is a jump discontinuity in* φ_* *at* $\xi = 0$ *of size*

$$\lim_{T\to\infty} \frac{1}{T} \int_0^T \frac{\mathrm{d}s}{\tilde{A}(s)},$$

which is nonzero when $1/\epsilon^2$ *is nonzero.*

(*b*) *For* $c = 0$, a *can be any value in* $[\varphi_-, \varphi_+]$.

Remark 5.1. Although for $c = 0$, a is any value in $[\varphi_-, \varphi_+]$, the error in a for wave speeds near zero is approximately

$$\lim_{T\to\infty} \frac{1}{T} \int_0^T \frac{\mathrm{d}s}{\tilde{A}(s)}.$$

Fig. 1 demonstrates behavior described by Theorem 5. In summary, for small wave speed c, spatial discretization causes large errors in both the parameter a and the solution profile. See [6] and [8] for more on this case.

5.3. Temporal discretization of Eq. (3)

Applying linear multistep methods (in particular we will look at the BDF and theta methods) to (3) we now examine the behavior of $a(c)$ and φ for $|c| \to \infty$ and $|c| \to 0$. Starting with $|c| \to \infty$ we provide analytical and numerical results for linear multistep methods, the first six BDF methods and the theta method. When $|c| \to 0$, the equation has no time dependence and hence no error in a or Ψ. The overall effect of applying these discretization methods to the traveling waves of (1) is wave speedup, i.e. the speed of the traveling wave solution to the time discretized problem is larger than the speed of the traveling wave to the original problem for the same potential energy. Fig. 2 illustrates wave speedup.

5.3.1. Temporal discretization in the $|c| \to \infty$ limit

For each of the temporal discretizations presented in this section, we consider the following formulation for large wavespeed c. Assume $\Delta t > 0$ and let $\phi(\eta) = \Psi(\xi)$ with $\eta = \xi/c$. Then the traveling wave equations for linear multistep methods, (10), becomes

$$\sum_{j=0}^{k} \alpha_j \phi(\eta - j\Delta t) = \Delta t \sum_{j=0}^{k} \beta_j \left[\frac{\epsilon^2}{c^2} \ddot{\phi}(\eta - j\Delta t) - f(\phi(\eta - j\Delta t)) \right]. \tag{29}$$

Let $\phi_*(\eta)$ be defined as $\phi(\eta, c) \to \phi_*^{\pm}(\eta)$ as $c \to \pm\infty$. For $\ddot{\phi}(\eta) < \infty$, $\eta \in \mathbb{R}$, when $|c| \to \infty$, $(\epsilon^2 \Delta t/c^2) \to 0$ and (10) can be written as the delay equation

$$\sum_{j=0}^{k} \alpha_{k-j} \phi_*^{\pm}(\eta + j\Delta t) = -\Delta t \sum_{j=0}^{k} \beta_{k-j} f(\phi_*^{\pm}(\eta + j\Delta t)), \tag{30}$$

where we have shifted the independent variable by $k\Delta t$ which does not effect the problem since the equation has translational invariance for shifts of length Δt. Observe that for finite η,

$$\phi_*^{+}(\eta + \Delta t) = \lim_{c\to\infty} \phi(\eta + \Delta t) = \lim_{c\to\infty} \Psi(\xi + c\Delta t) = 1,$$

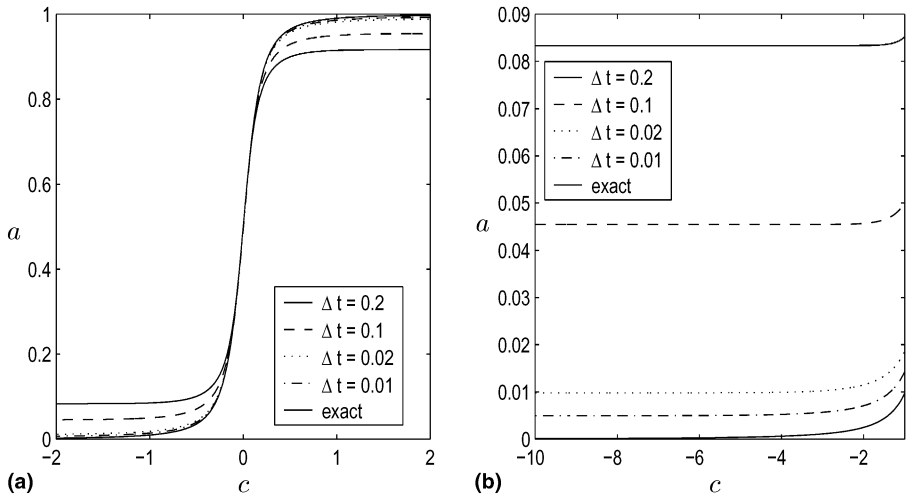

Fig. 2. Plots of $a(c)$ for the Backward Euler method with piecewise linear f. Plot (a) shows that the error occurs in the tails, when $|c|$ is large. Plot (b) is an enlargement of the tail of Plot (a). The first-order error term for Backward Euler is $\Delta t/2$.

$$\phi_*^-(\eta+\Delta t)=\lim_{c\to-\infty}\phi(\eta+\Delta t)=\lim_{c\to-\infty}\Psi(\xi+c\Delta t)=0,$$

and in fact $\phi_*^-(\eta,a)=1-\phi_*^+(\eta,1-a)$. Hence for this section we assume that $c>0$ and let $\phi_*\equiv\phi_*^+$.

Lemma 5.1. *Suppose $\alpha_k/\beta_k>0$. If $\phi_*(\eta_0)>a$ for some $\eta_0\in\mathbb{R}$, then $\phi_*(\eta)=1$ for all $\eta\geqslant\eta_0$.*

Proof. With $\alpha_k/\beta_k>0$ we may assume α_k and $\beta_k>0$. Then the right-hand side of (30) is nonnegative and the left-hand side is nonpositive for the nonlinearity f (2). Thus by (30), $\phi_*(\eta_0)=1$ and the conclusion follows for monotone nondecreasing solutions. □

Lemma 5.2. *Suppose η is such that $\phi_*(\eta)<a$ and $\phi_*(\eta+d)>a$ for $d\geqslant\Delta t$. Then $\phi_*(\eta)=1-(\beta_k\Delta t/(\alpha_k+\beta_k\Delta t))$.*

Proof. By Lemma 5.1 $\phi_*(\eta+d)=1$, the result follows directly from (30). □

Define the sequence $\{\phi_l\}_{l=-\infty}^{\infty}$ as

$$\phi_l=\begin{cases}1, & l>0,\\ 1-\frac{\beta_k\Delta t}{\alpha_k+\beta_k\Delta t}, & l=0,\\ -\frac{\sum_{j=1}^{k}\alpha_{k-j}\phi_{l+j}+\sum_{j=1}^{m}\beta_{k-j}\Delta t\phi_{l+j}}{\alpha_k+\beta_k\Delta t}, & l<0,\end{cases}\qquad l\in\mathbb{Z},\quad r\in(0,1),\tag{31}$$

where $m=\min(k,-l)$.

Theorem 6. *If the $\alpha_j,\beta_j,j=0,\ldots,k$ are such that $\alpha_k/\beta_k>0$ and such that $\{\phi_l\}$ is a monotone nondecreasing sequence where $\lim_{l\to-\infty}\phi_l=0$, then we have the following*:

(*a*) *The magnitude of the error in a as $|c|\to\infty$, $\lim_{|c|\to\infty}\mathrm{Err}_a$ is*

$$\frac{1}{2}\frac{\beta_k\Delta t}{\alpha_k+\beta_k\Delta t}=\frac{1}{2}\left[\frac{\beta_k}{\alpha_k}\Delta t-\frac{\beta_k^2}{\alpha_k^2}\Delta t^2+\frac{\beta_k^3}{\alpha_k^3}\Delta t^3-\cdots\right]=\frac{\beta_k}{\alpha_k}\frac{\Delta t}{2}\sum_{j=0}^{\infty}\left(-\frac{\beta_k}{\alpha_k}\Delta_t\right)^j,$$

a geometric series which is convergent for $\Delta t<\alpha_k/\beta_k$.

(*b*) *In addition*

$$\lim_{c\to\pm\infty}a(c)=\frac{1}{2}\pm\frac{\alpha_k}{2(\alpha_k+\beta_k\Delta t)}.$$

Remark 5.2. Thus $\lim_{|c|\to\infty}\mathrm{Err}_a$ for the k-step BDF methods is first order, not kth order, in Δt.

For the Backward Euler method

$$\lim_{|c|\to\infty}\mathrm{Err}_a=\frac{1}{2}\frac{\Delta t}{1+\Delta t}=\frac{\Delta t}{2}\sum_{j=0}^{\infty}(-\Delta t)^j\quad\text{and}\quad\lim_{|c|\to\pm\infty}a(c)=\frac{1}{2}\pm\frac{1}{2(1+\Delta t)}.$$

For the 2-step BDF method, where $\beta_0=\beta_1=0$, $\beta_2=2$, $\alpha_0=1$, $\alpha_1=-4$, and $\alpha_2=3$,

$$\lim_{c\to\pm\infty}a(c)=\frac{1}{2}\pm\frac{3}{2(3+2\Delta t)}\quad\text{and}\quad\lim_{|c|\to\infty}\mathrm{Err}_a=\frac{1}{2}\frac{2\Delta t}{3+2\Delta t}=\frac{\Delta t}{3}\sum_{j=0}^{\infty}\left(-\frac{2}{3}\Delta t\right)^j.$$

The first-order error coefficients, $\tilde{C}_1$, such that the leading order error term is of the form $\tilde{C}_1\Delta t$ in the $\lim_{|c|\to\infty} \mathrm{Err}_a$ for the BDF methods of order up to 6 are

k	1 = Backward Euler	2	3	4	5	6
$\tilde{C}_1$	1/2	1/3	3/11	6/25	30/137	30/147

Remark 5.3. For $k = 1$, the Backward Euler method, we see this agrees with the first-order error, $|\tilde{C}_1\Delta t| = \Delta t/2$ as $|c| \to \infty$ calculated in Section 4. Fig. 2 contains a set of $a(c)$ curves obtained numerical by solving the Backward Euler equation. We see they also agree with the above results.

For the theta method, $\theta \in [1/2, 1]$, where $k = 1$, and $\beta_1/\alpha_1 = \theta$,

$$\lim_{|c|\to\infty} \mathrm{Err}_a = \frac{1}{2}\frac{\theta\Delta t}{1+\theta\Delta t} = \frac{\theta\Delta t}{2}\sum_{j=0}^{\infty}(-\theta\Delta t)^j \quad \text{and} \quad a = \frac{1}{2}\frac{\theta\Delta t}{1+\theta\Delta t} = \frac{1}{2} - \frac{1}{2(1+\theta\Delta t)},$$

the $\lim_{|c|\to\infty} \mathrm{Err}_a$ is also *first order in* Δt.

Proof. (Theorem 6) We derive the results in a detailed fashion for $c \to \infty$, the results for $c \to -\infty$ follow the same analysis. For linear multistep methods $\phi_*(\eta)$, (30), is defined almost everywhere on $\mathbb{R}$ and contains jump discontinuities at intervals of Δt. Using the above lemmas, if we let the jumps occur when η is equal to an integer multiple of Δt, the solution profile ϕ_* is a series of disjoint steps whose values are $\phi_*(\eta) = \phi_*([l-r]\Delta t) \equiv \phi_l$, the elements of sequence (31), with ϕ_0 chosen so that a lies above ϕ_0 and below ϕ_1. For the Backward Euler method, the sequence $\phi_l = (1/(1+\Delta t))\phi_{l+1}$ for $l \leqslant 0$. The set of $\{\phi_l\}$ for the case when $c \to -\infty$ happens to be a geometric distribution.

To find the value of $\phi_*(\eta)$ at the jumps themselves, in particular, we want the value of a, we begin by considering the interface of $\phi(\eta)$ for (29) with c large but finite. Assume c is large enough so that the interface thickness ϵ/c is much smaller than the step length Δt, i.e., $\epsilon/c \ll \Delta t$. Then the profile $\phi(\eta)$ will have a step-like solution profile.

The set $\{\phi_l\}_{l=-\infty}^{\infty}$ found above (31) is a set of inflection points of the solution profile of (29). Using these points as boundary conditions we can solve

$$\frac{\epsilon^2\Delta t}{c^2}\sum_{j=0}^{k}\beta_{k-j}\ddot{\phi}(\eta+j\Delta t) = \sum_{j=0}^{k}[\alpha_{k-j}+\beta_{k-j}\Delta t]\phi(\eta+j\Delta t) - \sum_{j=0}^{k}\beta_{k-j}\Delta t, \quad n \in \mathbb{R},$$

with conditions $\phi(-\infty) = 0$ and $\phi(\infty) = 1$, by splitting the domain in subintervals of length Δt and solving for ϕ on each piece having conditions $\phi([2l-1]\Delta t/2) = \phi_l$, $\ddot{\phi}([2l-1]\Delta t/2) = 0$, $l \in \mathbb{Z}$. Although the solution found by this construction is not the solution to (29), it approaches it as $c \to \infty$. We further split each $[(l-1)\Delta t/2, (l+1)\Delta t/2]$ interval into the two subintervals $J^l_{\text{left}} = [(l-1)\Delta t/2, l\Delta t]$ and $J^l_{\text{right}} = [l\Delta t, (l+1)\Delta t/2]$, and define the matching conditions so that ϕ is continuously differentiable at each $\eta = l\Delta t$. Solving we find that for $l \in \mathbb{Z}$,

$$\phi(\eta) = \begin{cases} (\sum_{i=0}^{-l} A_{i1}[(\eta+i)\mathrm{e}^{-\lambda}]^i\mathrm{e}^{\lambda\eta} + B_{i1}[(\eta+i)\mathrm{e}^{\lambda}]^i\mathrm{e}^{-\lambda\eta}) + \phi_l, & \eta \in J^l_{\text{left}}, \\ (\sum_{i=0}^{-l} A_{i2}[(\eta+i)\mathrm{e}^{-\lambda}]^i\mathrm{e}^{\lambda\eta}) + B_{i2}[(\eta+i)\mathrm{e}^{\lambda}]^i\mathrm{e}^{-\lambda\eta}) + \phi_{l+1}, & \eta \in J^l_{\text{right}}, \end{cases}$$

where $\lambda = (c/\epsilon)\sqrt{((\alpha_k+\beta_k\Delta t)/\beta_k\Delta t)}$. When $l \geqslant 1$ and thus $\eta \geqslant \Delta t/2$, we know $\phi(\eta) = 1$. When $l = 0$, we find

$$\phi(\eta) = \begin{cases} A_{01}\mathrm{e}^{\lambda\eta} + B_{01}\mathrm{e}^{-\lambda\eta} + \frac{\alpha_k}{\alpha_k+\beta_k\Delta t}, & \eta \in [-\Delta t/2, 0], \\ A_{02}\mathrm{e}^{\lambda\eta} + B_{02}\mathrm{e}^{-\lambda\eta} + 1, & \eta \in [0, \Delta t/2], \end{cases}$$

with $\gamma = \lambda(\Delta t/2)$,

$$A_{02} = -B_{01} = \frac{\phi_1 - \phi_0}{2}\frac{e^{-\gamma} + e^{-3\gamma}}{e^{\gamma} - e^{-3\gamma}} \quad \text{and} \quad A_{01} = -B_{02} = \frac{\phi_1 - \phi_0}{2}\frac{e^{-\gamma} + e^{\gamma}}{e^{\gamma} - e^{-3\gamma}}.$$

We can continue to describe the solutions for each $l < 0$, but we stop here because we have what we need to find a. As $c \to \infty$, $\lambda \to \infty$, $\gamma \to \infty$, $A_{02} = -B_{01} \to 0$ and $A_{01} = -B_{02} \to ((\phi_1 - \phi_0)/2) = \frac{1}{2}(\beta_k \Delta t/(\alpha_k + \beta_k \Delta t))$, thus

$$\phi_*(\eta) = \begin{cases} \phi_0 = \frac{\alpha_k}{\alpha_k + \beta_k \Delta t}, & \eta \in (-\Delta t/2, 0), \\ \frac{\phi_1 + \phi_0}{2} = 1 - \frac{1}{2}\frac{\beta_k \Delta t}{\alpha_k + \beta_k \Delta t}, & \eta = 0, \\ \phi_1 = 1, & \eta \in (0, \Delta t/2). \end{cases}$$

Since the value of $\phi(0) = a$, as $c \to \infty$, $a \to \phi_*(0)$. A similar derivation for $c \to -\infty$ gives us $\lim_{c \to -\infty} a(c) = \frac{1}{2}(\beta_k \Delta t/(\alpha_k + \beta_k \Delta t))$. □

5.3.2. Temporal discretization in the $|c| \to 0$ limit

In this case both (3) and (10) have solution (4) and (5) with $c = 0$, hence no error.

5.4. Complete discretization – Backward Euler and rectangular spatial mesh

In this case we have a difference equation with no differential terms. Depending on the choice of $c, \Delta t, \Delta x_i$, $i = 1, \ldots, n$, and direction σ, the solution Ψ is either a dense or discrete set of values in $[0, 1]$. Suppose all of the delays in (17) are rationally related (as defined in Section 5.2.2), then the solution will be a discrete set of values in $[0, 1]$ and the domain, D, is a discrete set of $\mathbb{R}$. If any of the shifts are irrationally related, then the domain D is dense in $\mathbb{R}$. Since in both cases the solution profiles contain jump discontinuities we define

$$\Psi_\tau(\xi) = \tau \Psi(\xi^-) + (1 - \tau)\Psi(\xi^+) \quad \text{with } \tau \in [0, 1],$$

where $\Psi(\xi^\pm) \equiv \lim_{x \to \xi^\pm} \Psi(x)$ and shift the independent variable to obtain

$$-\Psi_\tau(\xi + c\Delta t) + \Psi_\tau(\xi) = \Delta t[\epsilon^2 L_T \Psi_\tau(\xi) - f(\Psi_\tau(\xi))],$$

where L_T is given in (7). This equation holds for all $\xi \in \mathbb{R}$ including the values of ξ where there are discontinuities. Since typically wave profiles are thought of as maps $\Psi : \mathbb{R} \to \mathbb{R}$ this is how we will define the following solutions and we will discuss the restriction to their domain D as an remark. The solution profiles will form steps when $|c| \to \infty$ and when $|c| \to 0$. The difference between the two cases comes from whether the temporal or the spatial discretization dominates the behavior.

5.4.1. Complete discretization in the $|c| \to \infty$ limit

In this case, the temporal discretization dominates.

For $|c|$ is large we assume $\Delta t > 0$ and let $\phi(\eta) = \Psi_\tau(\xi)$ with $\eta = \xi/c$. Then (17) becomes

$$-\phi(\eta) + \phi(\eta - \Delta t) = \Delta t[\epsilon^2 L_\infty \phi(\eta - \Delta t) - f(\phi(\eta - \Delta t))], \tag{32}$$

where

$$L_\infty \phi(\eta) = \sum_{i=1}^{n} \left\{ \frac{1}{\Delta x_i^2} \left[\phi\left(\eta + \frac{\Delta x_i}{c}\sigma_i\right) + \phi\left(\eta - \frac{\Delta x_i}{c}\sigma_i\right) - 2\phi(\eta) \right] \right\}.$$

Theorem 7. *For $\Delta x_i, \sigma_i,\ i = 1, \ldots, n$ rationally related, the error in a and the value of a are the set valued quantities defined for $\tau \in [0,1]$ as*

$$\lim_{|c|\to\infty} \mathrm{Err}_a = \frac{\Delta t}{1+\Delta t}\left[\frac{1}{2} - (1-2\tau)\lim_{T\to\infty}\frac{1}{2T}\int_0^T 1/\hat{A}(s)\,\mathrm{d}s\right],$$

and

$$\lim_{c\to\pm\infty} a(c) = \phi(0,\tau) = \frac{1}{2} \pm \frac{1}{1+\Delta t}\left[\frac{1}{2} - \Delta t(1-2\tau)\lim_{T\to\infty}\frac{1}{2T}\int_0^T 1/\hat{A}(s)\,\mathrm{d}s\right],$$

where

$$\hat{A}(s) = \hat{A}(s, \Delta t, \{\Delta x_i\}_{i=1}^n) := 1 + 2\Delta t \sum_{i=1}^n \frac{\epsilon^2}{\Delta x_i^2}(1 - \cos(s\Delta x_i \sigma_i)).$$

Remark 5.4. The function a is set valued and bounded away from 0 and 1 if and only if all $\Delta x_i = 0$ for some $i \in \{1, \ldots, n\}$.

Proof. Looking at either (17) or (32) we see that as $c \to \infty$, the spatial shifts are infinitely smaller that the temporal shifts. Recall from (31) that the two uppermost steps of the Backward Euler discretization in the $c \to \infty$ limit are

$$\phi_0 = \frac{\Delta t}{1+\Delta t} \quad \text{and} \quad \phi_1 = 1.$$

We want a variation (the spatially discrete operator with infinitely small shifts) of the step profile of the Backward Euler version of (30) connecting ϕ_0 and ϕ_1. Recalling Lemma 5.1 we solve

$$0 = \frac{1}{\Delta t} + \sum_{i=1}^n \frac{\epsilon^2}{\Delta x_i^2}[\phi(\eta + \Delta x_i\sigma_i) + \phi(\eta - \Delta x_i\sigma_i) - 2\phi(\eta)] - \left[\frac{1}{\Delta t} + 1\right]\phi(\eta) + \left[\frac{1}{\Delta t} + H(\eta)\right],$$

with boundary values ϕ_0 and ϕ_1. The results of the theorem now follow using the same analysis used in Theorem 4. □

5.5. Complete discretization in the $|c| \to 0$ limit

In this case, the spatial discretization dominates. Using the techniques presented in [6], the upper value, a_+, and the lower, a_-, of the interval J_c are given formally by

$$a_\pm(c) = \lim_{\gamma\to 0^\pm}\left(\frac{1}{2} + \frac{1}{\pi}\int_0^\infty \frac{s\gamma + B(s)}{s(A^2(S) + [s\gamma - B(s)]^2)}\,\mathrm{d}s\right),$$

where

$$A(s) = 1 - 2\epsilon^2\left\{\sum_{i=1}^n \frac{1}{\Delta x_i^2}(\cos(s\sigma_i\Delta x_i) - 1)\right\} - \frac{1}{\Delta t}(\cos(sc\Delta t) - 1), \quad \text{and} \quad B(s) = \frac{1}{\Delta t}(\sin(sc\Delta t)).$$

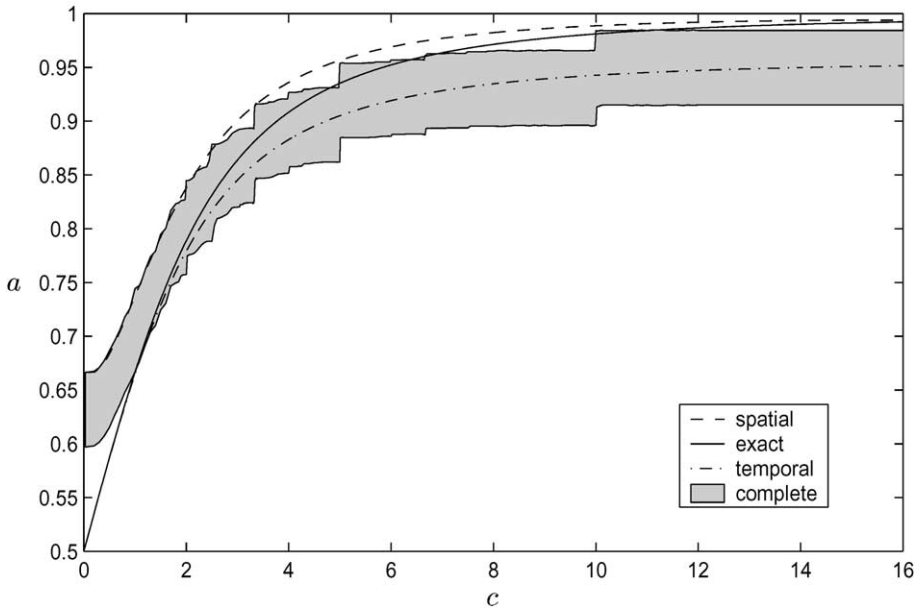

Fig. 3. A comparison of the $a(c)$ relations of the Backward Euler equation (10) [temporal], the rectangular spatial equation (7) [spatial], the complete discretizations with Backward Euler equation (17) [complete], and the original equation (4) [exact], for piecewise linear f, $\Delta t = 0.1$, $\epsilon^2 = 2$, $n = 2$, $\Delta x_1 = \Delta x_2 = \sqrt{2}$, and $\sigma = (1, 0)$. The values for this plot were obtained by solving each of the equations for a minimum of 1000 different values of c. The shaded region indicates the values of a for any $c \neq 0$.

To find the $|c| \to 0$ limits, one literally takes $\lim_{c \to 0^{\pm}} a_{\pm}(c)$. Fig. 3 illustrates the set valued nature of the function $a(c)$ (see Fig. 4).

6. Conclusion

We have analyzed the effect of appropriate temporal discretizations and uniform spatial discretization on traveling wave solutions of reaction–diffusion PDEs with piecewise linear reaction term. Our approach has been that of applying the discretization scheme to the original PDE and then analyzing the traveling wave equations that result from applying a traveling wave assumption. We have provided an analysis of the error in the waveform and (a, c) curve to first approximation that could prove useful in choosing time/space step sizes to minimize errors in the detuning parameter a and in the waveform. Generalizations to other models, for instance phase field models, appear possible. In general, we found that the effect of spatial discretization is most pronounced for wave speeds near zero resulting in pinning of waveforms and for temporal discretizations the effect is predominantly at large wave speeds and results in a possible constraint on the values of the detuning parameter a for which there will be traveling waves. These two effects both occur for complete discretizations and in this case the (a, c) curve becomes set valued even for $c \neq 0$, implying nonuniqueness in the (a, c) relationship.

While shown here for a particular nonlinearity, these results show the care that needs to be taken when solving bistable parabolic PDEs with relatively sharp interface motion using finite difference methods. Often of interest in systems of such PDEs, such as in phase field modeling, is anisotropic motion of the interface of the PDE (leading to such phenomena as dendritic growth). Finite differencing can both create and enhance such effects.

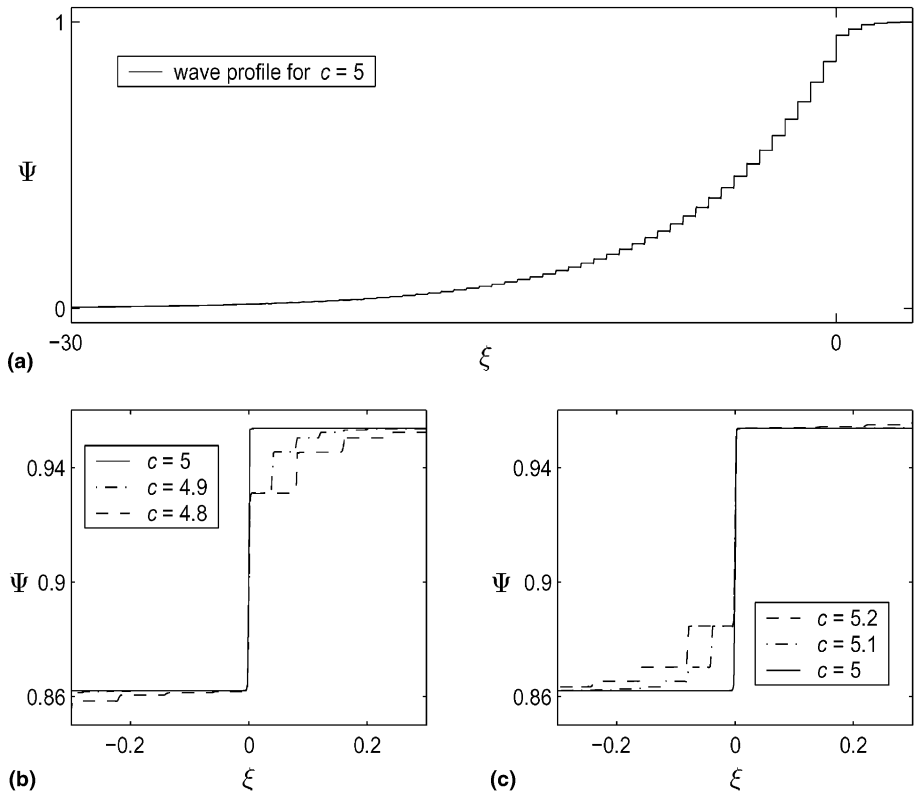

Fig. 4. In this plot we illustrate why the $a(c)$ plot for the complete discretization appearing in Fig. 3 has steps. We focus on the 'jump' which appears at $c = 5$. Plots (a), (b), and (c) are wave profiles $\Psi(\xi)$ for the complete discretization with nonlinearity, f, $\Delta t = 0.1$, $\epsilon^2 = 2$, $n = 2$, and $\Delta x_1 = \Delta x_2 = \sqrt{2}$. Recall that the value of $a = \Psi(0)$. Plot (a) is $\Psi(\xi)$ when the wave speed $c = 5$. Plots (b) and (c) are a magnification about $\xi = 0$ and illustrate how the step in the solution profiles at $\xi = 0$ 'jumps' as c increases though $c = 5$.

Acknowledgements

The authors would like to thank Paul Martin for discussions that led to Theorem A.1.

Appendix A

Theorem A.1. *For m a positive integer and n a nonnegative integer satisfying $n < 2m$ consider the integrals*

$$I_{mn} := \int_0^\infty \frac{x^{2n}}{(x^2+a^2)^m (x^2+b^2)^m}\,\mathrm{d}x \tag{A.1}$$

for nonnegative real numbers a and b not both zero. Then for $m = 1, 2, \ldots,$

$$I_{mm} = \pi \frac{c_m}{(a+b)^{2m-1}} \quad \text{and} \quad I_{m,m-1} = \frac{\pi}{ab}\frac{c_m}{(a+b)^{2m-1}}, \tag{A.2}$$

where

$$c_{m+1} = c_1 \frac{(2m)!}{2^{2m}(m!)^2}, \quad m = 1, 2, \ldots,$$

with $c_1 = \frac{1}{2}$. *Furthermore, for* $m = 2, 3, \ldots$

$$I_{m,m+1} = \frac{\pi}{(a+b)^{2m-1}}\left[(c_{m-1} - c_m)(a+b)^2 + c_m ab\right] \quad \textit{and} \quad I_{m,m-2} = \frac{I_{m,m+1}}{a^3 b^3}. \tag{A.3}$$

Proof. Induct on m and n starting with

$$I_{10} = \frac{\pi}{2ab}\frac{1}{a+b} \quad \text{and} \quad I_{11} = \frac{\pi}{2}\frac{1}{a+b}$$

using the identities

$$\frac{\partial^2 I_{mn}}{\partial a\, \partial b} = 4abm^2 I_{m+1,n}, \tag{A.4}$$

$$I_{m,n+2} = I_{m-1,n} - (a^2 + b^2) I_{m,n+1} - a^2 b^2 I_{mn}, \quad m = 2, 3, \ldots, \ n = 0, \ldots, 2m-3. \qquad \square \tag{A.5}$$

Remark A.1. Further formulas for admissible (m, n) may be derived in a similar fashion.

We write the polynomial of s given by $A^2(s) + c^2 s^2 \equiv \epsilon^4 s^4 + (2\epsilon^2 + c^2)s^2 + 1$ for $\epsilon > 0$ and $c \neq 0$ as $\epsilon^4(s^2 - \alpha_1)(s^2 - \alpha_2)$ where

$$\alpha_1 = \frac{-(c^2 + 2\epsilon^2) + c\sqrt{c^2 + 4\epsilon^2}}{2\epsilon^4}, \quad \alpha_2 = \frac{-(c^2 + 2\epsilon^2) - c\sqrt{c^2 + 4\epsilon^2}}{2\epsilon^4}. \tag{A.6}$$

If we let $a^2 = -\alpha_1$ and $b^2 = -\alpha_2$, then

$$I_{10} = \int_0^\infty \frac{\mathrm{d}s}{(s^2 - \alpha_1)(s^2 - \alpha_2)} = \frac{\epsilon^4 \pi}{2\sqrt{c^2 + 4\epsilon^2}}, \quad I_{11} = \frac{\epsilon^2 \pi}{2\sqrt{c^2 + 4\epsilon^2}}, \tag{A.7}$$

$$\begin{aligned} I_{20} &= \frac{\epsilon^{12}\pi}{4(c^2 + 4\epsilon^2)^{3/2}}\left[\frac{c^2 + 4\epsilon^2}{\epsilon^4} + \frac{1}{\epsilon^2}\right], \quad I_{21} = \frac{\epsilon^8 \pi}{4(c^2 + 4\epsilon^2)^{3/2}}, \\ I_{22} &= \frac{\epsilon^6 \pi}{4(c^2 + 4\epsilon^2)^{3/2}}, \quad I_{23} = \frac{\epsilon^6 \pi}{4(c^2 + 4\epsilon^2)^{3/2}}\left[\frac{c^2 + 4\epsilon^2}{\epsilon^4} + \frac{1}{\epsilon^2}\right]. \end{aligned} \tag{A.8}$$

These types of integrals are used to compute the $\tilde{C}_j$, $j = 1, 2, \ldots$, while to compute the C_j the following integrals are required

$$I^s_{mn}(\xi) := \int_0^\infty \frac{x^{2n+1}\sin(x\xi)}{(x^2 + a^2)^m (x^2 + b^2)^m}\,\mathrm{d}x \tag{A.9}$$

and

$$I^c_{mn}(\xi) := \int_0^\infty \frac{x^{2n}\cos(x\xi)}{(x^2+a^2)^m(x^2+b^2)^m}\,\mathrm{d}x. \tag{A.10}$$

These integrals also satisfy the identities (A.4) and (A.5) and we tabulate some that we employ below.

$$\begin{aligned} I^c_{10}(\xi) &= \frac{\epsilon^6\pi}{2c\sqrt{c^2+4\epsilon^2}}\left[\sqrt{-\alpha_2}\mathrm{e}^{-\sqrt{-\alpha_1}|\xi|} - \sqrt{-\alpha_1}\mathrm{e}^{-\sqrt{-\alpha_2}|\xi|}\right], \\ I^c_{11}(\xi) &= \frac{\epsilon^4\pi}{2c\sqrt{c^2+4\epsilon^2}}\left[\sqrt{-\alpha_2}\mathrm{e}^{-\sqrt{-\alpha_2}|\xi|} - \sqrt{-\alpha_1}\mathrm{e}^{-\sqrt{-\alpha_1}|\xi|}\right], \end{aligned} \tag{A.11}$$

$$I^s_{10}(\xi) = \frac{\epsilon^4\pi}{2c\sqrt{c^2+4\epsilon^2}}\left[\mathrm{e}^{-\sqrt{-\alpha_1}|\xi|} - \mathrm{e}^{-\sqrt{-\alpha_2}|\xi|}\right], \tag{A.12}$$

$$\begin{aligned} I^c_{20}(\xi) = {} & \frac{\epsilon^8\pi}{4c^2(c^2+4\epsilon^2)}\left[\mathrm{e}^{-\sqrt{-\alpha_1}|\xi|}\left(\frac{1}{(\sqrt{-\alpha_1})^3}+\frac{|\xi|}{(\sqrt{-\alpha_1})^2}\right)\right. \\ & \left.+\,\mathrm{e}^{-\sqrt{-\alpha_2}|\xi|}\left(\frac{1}{(\sqrt{-\alpha_2})^3}+\frac{|\xi|}{(\sqrt{-\alpha_2})^2}\right)\right] \\ & +\frac{\epsilon^{12}\pi}{c^3(c^2+4\epsilon^2)^{3/2}}\left[\mathrm{e}^{-\sqrt{-\alpha_2}|\xi|}\left(\frac{1}{\sqrt{-\alpha_2}}\right)-\mathrm{e}^{-\sqrt{-\alpha_1}|\xi|}\left(\frac{1}{\sqrt{-\alpha_1}}\right)\right], \end{aligned} \tag{A.13}$$

$$\begin{aligned} I^c_{21}(\xi) = {} & \frac{\epsilon^8\pi}{4c^2(c^2+4\epsilon^2)}\left[\mathrm{e}^{-\sqrt{-\alpha_1}|\xi|}\left(\frac{1}{(\sqrt{-\alpha_1})}-|\xi|\right)+\mathrm{e}^{-\sqrt{-\alpha_2}|\xi|}\left(\frac{1}{(\sqrt{-\alpha_2})}-|\xi|\right)\right] \\ & +\frac{\epsilon^{12}\pi}{c^3(c^2+4\epsilon^2)^{3/2}}\left[\mathrm{e}^{-\sqrt{-\alpha_2}|\xi|}(-\sqrt{-\alpha_2})-\mathrm{e}^{-\sqrt{-\alpha_1}|\xi|}(-\sqrt{-\alpha_1})\right], \end{aligned}$$

$$\begin{aligned} I^c_{22}(\xi) = {} & \frac{\epsilon^8\pi}{4c^2(c^2+4\epsilon^2)}\left[\mathrm{e}^{-\sqrt{-\alpha_1}|\xi|}\left(-3\sqrt{-\alpha_1}+|\xi|(\sqrt{-\alpha_1})^2\right)\right. \\ & \left.+\,\mathrm{e}^{-\sqrt{-\alpha_2}|\xi|}(-3\sqrt{-\alpha_2}+|\xi|(\sqrt{-\alpha_2})^2)\right] \\ & +\frac{\epsilon^{12}\pi}{c^3(c^2+4\epsilon^2)^{3/2}}\left[\mathrm{e}^{-\sqrt{-\alpha_2}|\xi|}(\sqrt{-\alpha_2})^3-\mathrm{e}^{-\sqrt{-\alpha_1}|\xi|}(\sqrt{-\alpha_1})^3\right], \end{aligned} \tag{A.14}$$

$$\begin{aligned} I^c_{23}(\xi) = {} & \frac{\epsilon^8\pi}{4c^2(c^2+4\epsilon^2)}\left[\mathrm{e}^{-\sqrt{-\alpha_1}|\xi|}(5(\sqrt{-\alpha_1})^3-|\xi|(\sqrt{-\alpha_1})^4)\right. \\ & \left.+\,\mathrm{e}^{-\sqrt{-\alpha_2}|\xi|}(5(\sqrt{-\alpha_2})^3-|\xi|(\sqrt{-\alpha_2})^4)\right] \\ & +\frac{\epsilon^{12}\pi}{c^3(c^2+4\epsilon^2)^{3/2}}\left[\mathrm{e}^{-\sqrt{-\alpha_2}|\xi|}(-\sqrt{-\alpha_2})^5-\mathrm{e}^{-\sqrt{-\alpha_1}|\xi|}(-\sqrt{-\alpha_1})^5\right], \end{aligned}$$

$$
\begin{aligned}
I^s_{20}(\xi) &= \frac{\epsilon^8\pi}{4c^2(c^2+4\epsilon^2)}\left[e^{-\sqrt{-\alpha_1}|\xi|}\left(\frac{\xi}{(\sqrt{-\alpha_1})}\right)+e^{-\sqrt{-\alpha_2}|\xi|}\left(\frac{\xi}{(\sqrt{-\alpha_2})}\right)\right]\\
&\quad+\frac{\epsilon^{12}\pi}{c^3(c^2+4\epsilon^2)^{3/2}}\left[e^{-\sqrt{-\alpha_2}|\xi|}-e^{-\sqrt{-\alpha_1}|\xi|}\right],\\
I^s_{21}(\xi) &= \frac{\epsilon^8\pi}{4c^2(c^2+4\epsilon^2)}\left[e^{-\sqrt{-\alpha_1}|\xi|}(2-\sqrt{-\alpha_1}\xi)+e^{-\sqrt{-\alpha_2}|\xi|}(2-\sqrt{-\alpha_2}\xi)\right]\\
&\quad+\frac{\epsilon^{12}\pi}{c^3(c^2+4\epsilon^2)^{3/2}}\left[-e^{-\sqrt{-\alpha_2}|\xi|}(\sqrt{-\alpha_2})^2+e^{-\sqrt{-\alpha_1}|\xi|}(\sqrt{-\alpha_1})^2\right],
\end{aligned}
\tag{A.15}
$$

$$
\begin{aligned}
I^s_{22}(\xi) &= \frac{\epsilon^8\pi}{4c^2(c^2+4\epsilon^2)}\left[e^{-\sqrt{-\alpha_1}|\xi|}(-4(\sqrt{-\alpha_1})^2+\xi(\sqrt{-\alpha_1})^3)\right.\\
&\quad\left.+e^{-\sqrt{-\alpha_2}|\xi|}(-4(\sqrt{-\alpha_2})^2+\xi(\sqrt{-\alpha_2})^3)\right]\\
&\quad+\frac{\epsilon^{12}\pi}{c^3(c^2+4\epsilon^2)^{3/2}}\left[e^{-\sqrt{-\alpha_2}|\xi|}(\sqrt{-\alpha_2})^4-e^{-\sqrt{-\alpha_1}|\xi|}(\sqrt{-\alpha_1})^4\right].
\end{aligned}
\tag{A.16}
$$

References

[1] K.A. Abell, C.E. Elmer, A.R. Humphries, E.S. Van Vleck, Computation of mixed type functional differential boundary value problems, 2001 (submitted).
[2] C.G. Aronson, W.F. Weinberger, Multidimensional nonlinear diffusion arising from population genetics, Adv. Math. 30 (1978) 33–76.
[3] R.J. Braun, B.T. Murray, Adaptive phase-field computations of dendritic crystal growth, J. Crystal Growth 174 (1997) 41–53.
[4] S.N. Chow, J. Mallet-Paret, W. Shen, Traveling waves in lattice dynamical systems, J. Differ. Equations 149 (1998) 248–291.
[5] J.W. Cahn, Theory of crystal growth and interface motion in crystalline materials, Acta Met. 6 (1960) 554–561.
[6] J.W. Cahn, J. Mallet-Paret, E.S. Van Vleck, Traveling wave solutions for systems of ODEs on a two-dimensional spatial lattice, SIAM J. Appl. Math. 59 (1999) 455–493.
[7] D.B. Duncan, M.A.M. Lynch, Jacobi iteration in implicit difference schemes for the wave equation, SIAM J. Numer. Anal. 28 (1991) 1661–1679.
[8] C.E. Elmer, E.S. Van Vleck, Analysis and computation of traveling wave solutions of bistable differential–difference equations, Nonlinearity 12 (1999) 771–798.
[9] C.E. Elmer, E.S. Van Vleck, Traveling waves solutions for bistable differential–difference equations with periodic diffusion, SIAM J. Appl. Math. 61 (2001) 1648–1679.
[10] C.E. Elmer, E.S. Van Vleck, Existence of monotone traveling fronts for BDF discretizations of bistable reaction–diffusion equations, J. Dyn. Continuous Discr. Impulsive Systems 10A (2002) 389–402.
[11] C.E. Elmer, E.S. Van Vleck, Dynamics of monotone traveling fronts for discretizations of Nagumo PDEs, 2002 (submitted).
[12] J.A. Feroe, Existence and stability of multiple impulse solutions of a nerve equation, SIAM J. Appl. Math. 42 (1982) 235–246.
[13] P.C. Fife, J.B. McLeod, The approach of solutions of nonlinear diffusion equations to travelling front solutions, Arch. Rat. Mech. Anal. 65 (1977) 335–361.
[14] E. Hairer, G. Wanner, Solving Ordinary Differential Equations II, Springer-Verlag, Berlin, 1991.
[15] J.K. Hale, S.M. Verduyn Lunel, Introduction to Functional Differential Equations, Springer-Verlag, New York, NY, 1993.
[16] A.C. Hindmarsh, LSODE and LSODI, two new initial value ordinary differential equation solvers, ACM–SIGNUM Newslett. 15 (1980) 10–11.
[17] J.P. Keener, Propagation and its failure in coupled systems of discrete excitable cells, SIAM J. Appl. Math. 47 (1987) 556–572.
[18] J.P. Keener, The effects of discrete gap junction coupling on propagation in myocardium, J. Theor. Biol. 148 (1991) 49–82.
[19] J. Keener, J. Sneed, Mathematical Physiology, Springer-Verlag, New York, NY, 1998.
[20] J. Mallet-Paret, The Fredholm alternative for functional differential equations of mixed type, J. Dyn. Differ. Equations 11 (1999) 1–48.

[21] J. Mallet-Paret, The global structure of traveling waves in spatially discrete dynamical systems, J. Dyn. Differ. Equations 11 (1999) 49–128.
[22] H. McKean, Nagumo's equation, Adv. Math. 4 (1970) 209–223.
[23] J. Nagumo, S. Arimoto, S. Yoshizawa, An active pulse transmission line simulating nerve axon, Proc. List. Radio Eng. 50 (1964) 2061–2070.
[24] L.R. Petzold, A description of DASSL: a differential/algebraic system solver, in: Proceedings of the IMACS World Congress, Montreal, Canada, 1982.
[25] L.R. Petzold, Automatic selection of of methods for solving still and non-stiff systems of ordinary differential equations, SIAM J. Sci. Stat. Comp. 4 (1983) 136–148.
[26] J. Rinzel, J.B. Keller, Traveling wave solutions of a nerve conduction equation, Biophys. J. 13 (1973) 1313–1337.
[27] A.M. Stuart, A.R. Humphries, Dynamical Systems and Numerical Analysis, Cambridge University Press, Cambridage, UK, 1996.
[28] W.-P. Wang, Multiple Impulse Solutions to McKean's caricature of the nerve Equation. I – existence, Comm. Pure Appl. Math. 41 (1988) 71–103.
[29] W.-P. Wang, Multiple impulse solutions to McKean's caricature of the nerve Equation. II. Stability, Comm. Pure Appl. Math. 41 (1988) 997–1025.
[30] S.-L. Wang, R.F. Sekerka, Algorithms for phase field computation of the dendritic operating state at large supercoolings, J. Comp. Phys. 127 (1996) 110–117.
[31] S.-L. Wang, R.F. Sekerka, A.A. Wheeler, B.T. Murray, S.R. Coriell, R.J. Braun, G.B. McFadden, Thermodynamically-consistent phase-field models for solidification, Phys. D 69 (1993) 189–200.
[32] H.F. Weinberger, Long-time behavior of a class of biological models, SIAM J. Math. Anal. 13 (1982) 353–396.
[33] H.F. Weinberger, Genetic wave propagation. Convex sets, and semi-infinite programming, in: C.V. Coffman, G.J. Fix (Eds.), Constructive Approaches to Mathematical Models, Academic Press, New York, 1979, pp. 293–317.
[34] B. Zinner, Stability of traveling wavefronts for the discrete Nagumo equation, SIAM J. Math. Anal. 22 (1991) 1016–1020.
[35] B. Zinner, Existence of traveling wavefront solutions for the discrete Nagumo equation, J. Differ. Equations 96 (1992) 1–27.